HHS Public Access

Author manuscript

Magn Reson Med. Author manuscript; available in PMC 2019 March 01.

Published in final edited form as:

Magn Reson Med. 2018 March ; 79(3): 1293–1303. doi:10.1002/mrm.26764.

Improved respiratory self-navigation for 3D radial acquisitions through the use of a "pencil-beam" 2D-T_2-Prep in free-breathing, whole-heart coronary MRA

A. J. Coristine[1,2,*], **J. Chaptinel**[2], **G. Ginami**[2], **G. Bonanno**[2], **S. Coppo**[2], **R. B. van Heeswijk**[2], **D. Piccini**[2,3], and **M. Stuber**[2,4]

[1]Department of BioMedical Engineering, Case Western Reserve University (CWRU), Cleveland, Ohio, USA [2]Department of Radiology, University Hospital (CHUV) / University of Lausanne (UNIL), Lausanne, VD, Switzerland [3]Advanced Clinical Imaging Technology, Siemens Healthcare, Lausanne, Switzerland [4]CardioVascular Magnetic Resonance (CVMR) research centre, Centre for BioMedical Imaging (CIBM), Lausanne, VD, Switzerland

Abstract

Purpose—In respiratory self-navigation (SN), signal from static structures, such as the chest wall, may complicate motion detection or introduce post-correction artefacts. Suppressing signal from superfluous tissues may therefore improve image quality. We thus test the hypothesis that SN whole-heart coronary magnetic resonance angiography (MRA) will benefit from an outer-volume suppressing "2D-T_2-Prep" and present both phantom and *in vivo* results.

Methods—A 2D-T_2-Prep and a conventional T_2-Prep were used prior to a free-breathing 3D-radial SN sequence. Both techniques were compared by imaging a home-built moving cardiac phantom and by performing coronary MRA in 9 healthy volunteers. Reconstructions were performed using both a reference-based and a reference-independent approach to motion tracking, along with several coil combinations. Signal-to-noise ratio (SNR) and contrast-to-noise ratio (CNR) were compared, along with vessel sharpness (VS).

Results—In phantoms, using the 2D-T_2-Prep increased SNR by 16-53%, mean VS by 8%, and also improved motion tracking precision was achieved. In volunteers, SNR increased by an average of 29-33% in the blood pool and 15-25% in the myocardium, depending on the choice of reconstruction coils and algorithm, and VS increased by 34%.

Conclusion—A 2D-T_2-Prep significantly improves image quality in both phantoms and volunteers when performing SN coronary MRA.

Keywords

2D; Adiabatic; Coronary; Inner Volume; Iterative; Self-Navigation; T_2-Prep

[*]Corresponding author: Andrew J. Coristine, Case Western Reserve University, Wickenden Building Room 516, 2071 Martin Luther King Jr. Drive, Cleveland, Ohio, 44106-7297, USA, < andrew.coristine@gmail.com>.

Introduction

In traditional whole-heart magnetic resonance angiography (MRA), cardiac and respiratory motion make it challenging to both rapidly and accurately acquire high-resolution images (1-3). To minimize the effects of *cardiac* motion, data acquisition is most often timed to coincide with quiescent periods of the cardiac cycle (i.e. end-systole or mid-diastole) (4,5), through electrocardiography (ECG) triggering or self-gated methods (6-12). Conversely, minimizing the effects of the *respiratory* motion is more problematic. Most often, this is achieved by discarding and reacquiring data collected during unfavourable respiratory phases, which are identified through the use of diaphragmatic respiratory navigators (13). While several innovative strategies have been proposed to improve on diaphragmatic navigators (14-16), navigator-based approaches nonetheless remain highly inefficient. Additionally, these approaches also suffer from problems such as respiratory drift (17), sub-optimal navigator positioning (18), temporal delays (19), hysteresis effects (20), operator dependence, and the fact that diaphragmatic respiratory motion is only an approximation of cardiac respiratory motion (21).

A more accurate and time-efficient approach may be to directly track the heart's respiratory motion and to then perform motion correction on data acquired during non-ideal respiratory phases. As a displacement in image space is equal to a phase shift in k-space (22), one may compensate for the respiratory displacement of the heart by adding a corresponding phase shift to data acquired during any given respiratory position. In turn, this allows for 100% scan efficiency, as data may be used regardless of respiratory position. While Cartesian imaging nonetheless remains the reference standard, self-navigated approaches (23-26) such as these have found widespread application with several notable developments (27-35), and have even becoming routine in certain clinical settings (36-39).

In order to identify the aforementioned respiratory motion, one implementation collects a one dimensional (1D) superior-inferior (SI) projection at the start of each ECG-triggered acquisition window (23,24). In that approach, the blood pool is identified as a hyperintense structure and by tracking its displacement, respiratory motion can be identified and used for motion correction. While highly promising, these self-navigation (SN) techniques nonetheless remain imperfect.

One major issue is that static structures, such as the chest wall and arms, make it difficult to reliably track the position of the blood pool. This may be particularly problematic in female or obese patients, where increased chest tissue can interfere with blood pool tracking. Even when motion detection is successful, rigid motion correction may subsequently introduce artefacts when applied to static structures. That is, when compensating for respiratory motion, one effectively turns non-moving structures into moving ones. In Cartesian acquisitions, this artificial motion can result in blurring and ghosting, whereas in radial acquisitions, this may also present as streaking (40). This advances the hypothesis that suppressing signal from these static tissues may significantly improve image quality in SN.

Several inner volume selection (IVS) / outer volume suppression (OVS) techniques have been proposed (41-45), though many rely on lengthy excitation or preparation schemes.

Conversely, a "2D-T_2-Prep" (46) has recently been introduced which incorporates a 2D selective excitation pulse into a T_2 Preparation module. Prior to imaging, this technique adds T_2-weighting to a cylindrical region of tissue, while simultaneously spoiling signal elsewhere.

While this technique has been reported for navigator-based coronary imaging (46,47), it has not yet been tested with whole-heart self-navigated 3D radial MRA. Since whole-heart MRA is frequently T_2-prepared, replacing a conventional T_2-Prep with this 2D-T_2-Prep should add no additional time requirements. Additionally, by suppressing signal from static tissues, image quality should improve, as should motion tracking. Thus, the 2D-T2-Prep provides a useful tool for exploring the previously unreported idea that outer volume suppression can improve self-navigation image acquisition.

In this study, we therefore test the hypothesis that SN 3D radial coronary MRA will benefit from the introduction of an outer volume suppressing 2D-T_2-Prep, as compared to a conventional T_2-Prep. A new moving heart phantom is introduced to test this hypothesis, and whole-heart MRA is performed 9 healthy volunteers. Possible confounders are also investigated by exploring multiple published motion tracking techniques and differing coil combinations.

Methods

Self-Navigation

A previously described (48) prototype 3D radial trajectory, specifically adapted to perform self-navigation, was used for data acquisition. During each heartbeat, this ECG-triggered sequence collects several readouts, collectively known as an interleaf. In each interleaf, acquisition begins with an initial superior-inferior (SI) projection, which is used to determine the position of the cardiac blood pool. This is followed by a series of Koosh ball-like 3D radial readouts. Beginning from the top of a hypothetical sphere encompassing all of k-space, projections crossing through the center of k-space are acquired. Each projection is rotated along the azimuth, and again along the altitude, such that the sum of all projections in a given interleaf forms a phyllotactic 3D spiral (48). While each spiral interleaf follows the same pattern, subsequent interleaves are rotated by the golden angle about the z-axis. This has the effect of uniformly sampling k-space regardless of the number of projections acquired, while simultaneously minimizing eddy currents (Figure 1).

After a full dataset is acquired, the relative position of the heart along the SI direction is calculated for each interleaf. Respiratory motion estimation was first performed in an automated, reference-based approach (24). With this approach, an individual SI projection is chosen as respiratory reference (30), and the relative displacement of all the other acquired projections with respect to the reference position is calculated. While this reference-based approach is the current gold-standard, a reference-independent, iterative approach to SN has recently been introduced (49) and has been shown to improve vessel sharpness in coronary imaging relative to the non-iterative, reference-based approach in patient studies. Motion detection was also performed with this new reference-independent technique, which operates by iteratively minimizing the residual respiratory displacement throughout the

complete series of SI projections (i.e. without requiring the selection of a specific respiratory reference position), so as to determine if the potential improvements of the 2D-T_2-Prep were resulting only from an improved reference detection.

For both approaches (automated and iterative), the actual motion detection was performed by using the SI projection data from all available coils, or alternatively, by using an SI projection from a subset of coils closest to the heart (defined as the “best” coils in this manuscript). By restricting SI projection data to a subset of coils, one may potentially minimize the influence of static structures on cardiac motion detection. Thus, to determine if the benefits of the 2D-T_2-Prep's outer volume suppression can be replicated through coil elimination, SI projections from both coil strategies were examined. The “best” coils were manually selected after examining the signal contribution of each coil and visually selecting those where the coil image was primarily of the heart (in practice, this was most often the four central coils). As a displacement in image space is equal to a phase shift in k-space (22), the respiratory displacement of the heart is corrected for by adding a corresponding phase shift to that interleaf. Specifically, the linear phase for each readout is computed according to the detected shift and to the polar angle between the current readout and the SI orientation (23). The final, motion-corrected image can then reconstructed.

2D-T_2-Prep

A previously described T_2 preparation module (50), known as the 2D-T_2-Prep (46), was used prior to respiratory self-navigated image acquisition. Briefly, the 2D-T_2-Prep begins with a 2D selective excitation pulse (44,51,52), consisting of a jinc pulse played out with spiral gradients (53-55), which excites a cylinder of magnetization. By altering the radiofrequency (RF) pulse and gradient parameters, the diameter, location, and shape of the excitation profile may be adjusted. In this implementation, the 2D pulse properties were chosen to mimic the anatomy of the adult heart: a cylinder diameter of 12.0 cm, aliasing rings of diameter 48.0 cm, and a jinc-shaped RF pulse with five zero-crossings, to ensure uniform excitation (Figure 1). These values corresponded to a spiral trajectory with 15.6 turns, which on a clinical scanner with a gradient strength of 45 mT/m and a maximum slew rate of 200 T/m/s, results in a 5.8 ms RF pulse duration.

After this 2D pulse is played out, the excited signal decays according to the T_2 value of the associated tissue, being refocused with two hyperbolic secant adiabatic 180° pulses (56-58). This added T_2-weighting provides contrast between the high-T_2 blood pool and the low T_2-myocardium. A final, non-selective restoration pulse restores the transverse magnetization prior to the start of imaging. However, in the case of the 2D-T_2-Prep, this non-selective pulse also affects magnetization outside of the initially excited cylinder. As a result, while the cylinder is restored, the (formerly) longitudinal magnetization outside of the cylinder is rotated in the transverse plane, where it is then spoiled. As a result, only a cylinder of T_2-Prepared tissue remains at the start of imaging.

In these experiments, the 2D cylinder was applied along the bore of the magnet, which corresponded to the axis of motion in the moving phantom studies and the SI direction in volunteers (see below).

Moving Phantom

A custom, home-built moving cardiac phantom (Figure 2), inspired by Huber *et al.* (59), was constructed to compare the performance of the two pulses. A stepper motor, which rotates at a programmable rate, was used to drive a wooden pole sinusoidally in and out of the MRI bore. In turn, this moves a wheeled cart back and forth within the scanner. A commercially available K'NEX construction set (Hyper Space Training Tower, K'NEX Industries, Inc., Harfield, PA) was used to create a rigid frame around the moving cart, upon which a chest coil could be placed.

In these experiments, the cart was loaded with several phantoms, which had been doped to mimic the relaxation properties of the cardiac blood pool, fat, and myocardium. Additionally, a length of flexible tubing, with an inner diameter of 6 mm, was filled with a nickel sulfate solution (0.375% $NiSO_4$ w/w), to create a large, mock coronary artery. Several smaller phantoms, with varied relaxation properties, were also placed within the rigid K'NEX frame, to represent static structures within the body. Notably, several small baby oil (Johnson and Johnson, New Brunswick, NJ) phantoms were also placed underneath the chest coil, to represent static adipose tissue in the torso.

Phantom Experiments

The above described moving phantom was used to perform simulated free-breathing SN coronary MRA. To do so, an artificial ECG gating signal of 60 BPM was generated and a “respiratory” displacement of +/- 2 cm, with a frequency of 17 RPM, was programmed into the stepper motor. Images were collected on a 1.5 T clinical scanner (MAGNETOM Aera, Siemens Healthcare, Erlangen, Germany), using the 3D radial phyllotactic sequence described above, with a bSSFP readout, 18 channel chest coil and 12 channel spine coil, $(1.15\ mm)^3$ isotropic voxels, FoV $(220\ mm)^3$, matrix size 192^3, TE T_2-Prep = 40 ms, RF excitation angle 110°, 16 readouts/heartbeat, and TE/TR/T_{acq} = 1.82/3.63/58 ms. These experiments were repeated 5 times each for both a conventional adiabatic T_2-Prep and the 2D-T_2-Prep.

Motion tracking, correction, and reconstruction were attempted post-acquisition, using a commercial programming language (MATLAB 7.11, The MathWorks Inc., Natick, MA, United States) employing one of four possible strategies. Firstly, a previously described automated, reference-based segmentation approach (24) was used to identify the “blood pool” in the moving phantom by examining the SI projections. This was attempted using SI projections created from all coils, or created only from those coils closest to the blood pool (the “best” coils). In the moving phantom, this corresponded to only using the spinal coils for motion tracking. Motion correction was also attempted using an iterative approach (49), again using either all coils or only the “best” coils to identify the blood pool. The four strategies are thus defined, for convenience, as automated/iterative + all/best coils.

After reconstruction, signal-to-noise ratio (SNR) and contrast-to-noise ratio (CNR) were measured in the “blood” and “myocardium” of the phantom. Additionally, vessel sharpness % (VS) was measured in the mock coronary artery using the Soapbubble (60) visualization and analysis tool. SI projections were also analysed to determine the sharpness of the

phantom's "blood pool", which is delineated and tracked when performing motion correction (23,24,49). The maximum gradient between the "blood pool" and adjacent "tissue" was determined by examining each interleaf's SI projection, and the mean maximum gradient was calculated for both the conventional and the 2D-T_2-Prep. When possible (see Results), a paired two-tailed student's t-test was used to compare results from the conventional T_2-Prep +SN and the 2D-T_2-Prep+SN, with $P<0.05$ considered statistically significant.

The calculated motion shifts for each SI projection were also temporally aligned and then fit to a sine curve corresponding to the known motion of the moving phantom, using a least squares approach. Using the 60 BPM sampling rate, the root mean square error (RMSE) of the sine fit was determined for each T_2-Prep technique, given the known sinusoidal respiratory pattern of 17 RPM. The RMSE of the fit was then calculated for each repetition, and a paired two-tailed student's t-test (with unequal variance) was used to compare results, with $P<0.05$ considered statistically significant.

In vivo experiments

Free-breathing, ECG-gated, respiratory self-navigated, 3D radial whole-heart coronary MRA was performed in 9 healthy adult volunteers (4 female, 5 male), aged 25-34. All experiments were approved by the institutional review board, and written informed consent was obtained from each study participant. Imaging parameters were as per the phantom study above, with imaging taking place during the most quiescent mid-diastolic phase of each volunteer's cardiac cycle. This phase of quiescence was identified through a high-temporal resolution 4-chamber 2D cine image acquired at the start of each scanning session.

Motion tracking and reconstruction were performed using the same four technique combinations attempted during phantom imaging (automated/iterative + all/best coils). Depending on the volunteer, the "best" coils were either the four or six central anterior coils of the 18 channel chest coil, as described above (see Methods: Self-Navigation). After reconstruction, a region of interest (ROI) was selected in each of 3 tissues: blood, myocardium, and lung. For both T_2 preparation modules (2D/conventional), and for all four tracking techniques, the SNR and CNR of each tissue were calculated using the formula $SNR_{tissue}=S_{tissue}/\sigma_{lung}$ and $CNR=|S_{tissue1}-S_{tissue2}|/\sigma_{lung}$, where S is the average signal strength in the ROI and σ_{lung} is the standard deviation of the lung signal. The ROI from the lung was manually selected so as to be inside the area excited by the 2D-T_2-Prep, with visible blood vessels excluded, for use as ersatz "background" (45). After a multiplanar image reformat using Soapbubble (60), VS was measured in both the left and right coronary artery systems (LCA / RCA). These measurements were performed using the "best coils", and both the reference-dependent automated segmentation and the reference-independent iterative reconstruction techniques, for both the conventional and the 2D-T_2-Prep. As a additional assessment of image quality, two expert observers (8 and 22 years of experience) were blinded and evaluated the image quality of the coronary arteries in those data sets. First, a mask was applied to each volume, so that the observers were blinded as to whether the 2D-T_2-Prep or conventional T_2-Prep had been used (i.e. obscuring everything outside of the heart). Image sets were then presented in a random order and were scored on a consensus

basis, using a scale of 0-4, based on the visibility and sharpness of the entire coronary vasculature.

To determine statistical significance, a three-factor ANOVA with interaction test was first used to determine whether a difference existed between the protocols ($F>F_{crit}$, $P<0.05$), where the following variables were examined: automated/iterative reconstruction, all/best coils, and 2D/conventional T_2-Prep. Two factor-ANOVA (with interaction) was likewise performed for VS %. After establishing that a difference existed, a paired 2-tailed Student's t-test was used to compare the SNR and CNR from the conventional T_2-Prep+SN and the 2D-T_2-Prep+SN, with $P<0.05$ considered statistically significant.

Cartesian acquisitions

An additional 9 volunteers (5 female, 4 male), aged 23-35, were subsequently recruited and scanned with a more traditional Cartesian navigator- and ECG-gated sequence, to provide a reference standard. Sequence parameters were chosen to be similar of Sakuma *et al* (61), with 3D whole-heart centric-ordered segmented bSSFP sequence with a 280×280×120 mm^3 imaging volume, 160 slices (80 acquired), 256×256 matrix size (interpolated to 512×512), TE = 1.92 ms, TR = 297 ms, BW = 1085 Hz, 35 segments / heartbeat (3.8 ms echo spacing), RF excitation angle = 90°, T2-Prep TE = 50 ms, CHESS fat saturation, and a GRAPPA acceleration factor of 2 (24 reference lines).

Soapubble was then used to measure VS in both the right and left coronaries, and the above two expert observers evaluated the image quality of the vessels in those data sets, as described above. A one-factor ANOVA with interaction test was first used to determine whether a difference existed between the Cartesian and self-navigated (2D/conventional) results ($F>F_{crit}$, $P<0.05$), for both the left and right coronaries, using the best coils. ANOVA (with interaction) was likewise performed for VS %. After establishing that a difference existed, a paired 2-tailed Student's t-test was used to compare the Image Quality Assessment (IQA) and VS % between the Cartesian images, 2D-T2-Prep+SN, and conventional T_2-Prep +SN, with $P<0.05$ considered statistically significant.

Results

Phantom Experiments

In the moving phantom, all motion detection approaches (automated & iterative) and coil combinations (all & best) were successful when the 2D-T_2-Prep was used. However, when the conventional T_2-Prep was used, motion correction was less effective, as determined by visual inspection (see Supporting Figure S1) unless both a selected coil subset (the “best” coils) and the iterative motion detection approach were used together. However, even in the best coils + iterative case, the 2D-T_2-Prep still outperformed the conventional T_2-Prep, increasing blood SNR by 53% (58.5±2.4 vs. 23.6±2.1), myocardial SNR by 47% (23.6±1.5 vs 12.6±1.4), and VS by 7.5% (62.3±0.6 vs 58.0±0.8). Likewise, the mean signal gradient of the SI projections (Figure 3) increased by 10.8% (AU) when using the 2D-T_2-Prep (all $P<0.05$).

The sine fit was also superior when using the 2D-T_2-Prep. Specifically, when fitting the detected motion to a sine curve with a frequency equal to that of the moving phantom, the RMSE of the fit was between 0.3690 and 0.3882, with a mean value of 0.3763 (±0.008), for the 5 experiments that used the 2D-T_2-Prep. Conversely, when using the conventional T_2-Prep, the RMSE of the fit was between 0.5318 and 2.799, with a mean value of 1.293 (±0.952). Despite the high standard deviation of the conventional T_2-Prep (0.952), the decreased RMSE in the 2D-T_2-Prep was still statistically significant (P<0.05).

In Vivo Experiments

In volunteers, the 2D-T_2-Prep maintained high signal in the region targeted by the 2D-selective pulse, while exterior signal, in the chest, arms, and lungs, was clearly attenuated (Figure 4). High T_2-weighted contrast could also be observed between the blood pool and myocardium, and the coronary arterial system could be visualized and analysed (Figure 5). Consistent with these observations, a high blood-myocardium CNR was measured for both approaches, though the CNR of the 2D-T_2-Prep was significantly higher (37.3-46.1% improvement depending on protocol; see Table 1). Similar results were found for blood-lung CNR (13.7-14.1% improvement) and myocardium-lung CNR (4.1-4.4% improvement). As compared to the conventional T_2-Prep, the 2D-T_2-Prep also significantly improved the SNR of the blood pool (29.0-33.3% improvement) and the myocardium (14.9-25.3% improvement). Although the magnitude of the improvement varied, these improvements were always observed, and were always significantly different (all P<0.05 or better), regardless of the motion detection approach used, and regardless of the coil subsets selected (Table 1). Additionally, when analysing the RCA, VS increased by 34% (29.3±9.0 vs. 39.3±9.4) when using the 2D-T_2-Prep with an automated segmentation approach (P<0.002) and by 23% (33.7±7.3 vs. 41.2±6.7) when using the iterative reconstruction (P<0.01). In the LCA, VS increased by 21% (35.7±7.4 vs. 29.4±6.7) when using the 2D-T_2-Prep with an automated segmentation approach (P<0.02) and by 20% (36.7±7.0 vs. 30.6±6.6) when using the iterative reconstruction (P<0.02). An example can be seen in Figure 5, where the decreased background signal in the 2D-T_2-Prep leads to an increased conspicuity of the distal left coronary system.

In the blinded observer ratings of coronary image quality, 2D-T_2-Prep+SN increased the mean score by 64% (2.0±0.9vs 1.2±0.8) for an automated segmentation approach (P<0.05) and by 45% (1.9±0.7 vs. 1.3±0.9) when using the iterative reconstruction, though the latter result did not reach statistical significance (P=0.07).

Cartesian acquisitions

In the subsequent Cartesian acquisitions, the mean VS % in the LCA was 40.9±7.3. This was a non-significant 7% increase as compared to the 2D-T2-Prep+SN (p=0.15), and a significant 49% increase as compared to the conventional T2-Prep+SN (p<0.005). The mean VS % in the RCA was 51.4±11.5. This was a significant 28% increase as compared to the 2D-T2-Prep+SN (p<0.05), and a significant 59% increase as compared to the conventional T2-Prep+SN (p<0.002). Two representative images of the reformatted Cartesian acquisitions may be seen in Figure 5 (e,f).

In the observer ratings of Cartesian coronary image quality, the mean IQA score was 2.5±1.0. This was superior to all self-navigated scores, but only reached statistical significance when compared to the conventional T2-Prep [2D-T2-Prep: 2.0±0.9 ($p=0.25$) / 1.9±0.7 ($p=0.13$) iterative/automated; Conventional 1.2±0.8 ($p<0.01$) / 1.3±0.9 ($p<0.02$)] due to the higher threshold required for unpaired comparisons.

Discussion

As compared to a conventional T_2-Prep, the 2D-T_2-Prep significantly improved SNR, CNR, and VS % in both phantoms and volunteers, when performing self-navigated coronary MRA.

We posit that there are two main reasons for these improvements in image quality. Firstly, the suppression of extraneous signal, such as from the chest wall and arms, may make it easier to detect the respiratory position of the blood pool along the SI direction, making motion identification and tracking more accurate. As can be seen in Figures 3c and 3g, when static tissue signal is attenuated with the 2D-T_2-Prep, the blood pool is more clearly visualized and easier to identify. Evidence of this can also be seen by examining the mean gradient of the blood pool in the moving phantom, which was 10.8% sharper when using the 2D-T_2-Prep. As a sharper blood pool delineation presumably leads to improved blood pool identification, motion detection and correction may also be more accurate. Thus, artefacts due to insufficient motion correction are reduced. This is also corroborated by the improved quality of the moving phantom's sine fit when using the 2D-T_2-Prep, where the mean RMSE was significantly lower (0.3763) than with the conventional T_2-Prep. (1.293). In the non-2D case, the motion detection also visually appears to deviate from the expected sinusoidal motion of the moving phantom (Figure 3h). Conversely, no such deviation occurs in the 2D-T_2-Prep case (3d).

Secondly, in addition to better blood pool tracking, the 2D-T_2-Prep also leads to a reduction in streaking artefacts after motion correction. In part, this may be why the SNR increases were so dramatic in the phantom experiment results; background noise was far higher in the conventional T_2-Prep. Specifically, when rigid-body respiratory motion correction is applied to compensate for cardiac displacement, this effectively turns static tissues into moving ones. Signal from the arms and chest wall, which do not follow the same respiratory displacement pattern as the heart, becomes corrupted by the introduction of an incoherent motion “correction”. For the undersampled 3D radial phyllotactic self-navigation sequence being studied, this results in streaking artefacts and blurring across the image, increasing the apparent background signal. These artefacts decrease image quality, despite the improved scan efficiency of the self-navigation sequence. Thus, the SNR increase when using the 2D-T2-Prep should be viewed primarily as reduction in background noise and streaking artefacts, rather than an increase in signal.

Note that an important contribution to the above streaking artefacts is that only translational motion correction is performed. This incorrectly causes static tissues to appear to be moving (i.e. via the respiratory motion correction), causing streaking in this 3D radial sequence. Affine and non-rigid motion correction approaches might thus reduce the frequency, number,

and severity of such streaking artefacts, as in those cases, static tissues would no longer be artificially turned into “moving” ones (27). In turn, this would eliminate many of the problems that the 2D-T2-Prep attempts to resolve. In this work, such non-rigid motion correction approaches were not explored. Combining this approach with affine (28,62) and non-rigid (63) motion correction, or iterative reconstruction (35,64), may very well prove to be a highly promising strategy. It may even obviate the benefits of OVS. However, that this comparison was not attempted remains a limitation of this work.

It is nonetheless interesting to note that the 2D-T_2-Prep outperformed the conventional T_2-Prep for both the “all” and the “best” coil selections. Specifically, when using an SI projection for motion tracking, one might expect that by eliminating coils distant from the heart, blood pool tracking would improve. In effect, choosing the “best” coils might have the same effect as using a 2D-T_2-Prep. However, statistical analysis showed no significant difference between the “all” and “best” coils, in terms of SNR and CNR, whereas using the 2D-T_2-Prep (rather than the conventional T_2-Prep) did show a significant improvement in both.

Despite this, the motion tracking analysis did have specific weaknesses in the phantom experiments. In the moving phantom, although motion was periodic, it could not be guaranteed to be perfectly sinusoidal. For instance, a slight amount of drag, friction, or sliding might have resulted in motion that was imperfectly curved. Despite this possible flaw, motion tracking fidelity was still determined by the RMSE of a sine fit. Because of this intrinsic limitation, the RMSE values reported cannot be viewed as absolute measures of motion tracking accuracy. Instead, they should be viewed as relative indicators; while both may suffer from an unknown offset, or additional error, the more accurate technique should still be closer to a sine curve than one which incorrectly detects motion.

For the volunteer studies, a potential weakness is that inflow effects were not considered. As the 2D-T_2-Prep suppresses signal outside of the targeted region, one might expect some of the incoming blood (e.g. from the subclavian or pulmonary veins) to have decreased signal intensity. This may be particularly problematic in patients with high heart rates, as saturated blood will have less T_1 recovery time before entering the heart. While this effect was not seen in this study, it bears mentioning that none of the volunteers had a particularly high rate (all <75 bpm). In cardiac patients, heart rates may be elevated; thus, this potential limitation may be more significant in future studies.

Likewise, despite the apparent improvement of the 2D-T_2-Prep on image quality, there were several other limitations to this work as well. Firstly, although background signal suppression was effective, it remained imperfect outside of the region selected by the 2D-T_2-Prep. Based on previous investigations (46,65), we hypothesize that this may be related to B_1 inhomogeneity in the non-selective T_2-Prep restoration pulse (i.e. at the end of the T_2-Prep) or due to T_1 signal recovery after spoiling or during the radial signal readout train. It may also be because 2D selective excitation pulses are not perfect in practice. As such, the current implementation may be less effective than theoretically possible. In all of these cases, however, improving background suppression may lead to even greater SNR, CNR, and possibly VS improvements.

It may also be worth exploring other approaches to chest wall signal saturation. One example would be to explore a modified version of our 2D-T_2-Prep, such as the one recently proposed by Luo et al. (66). That version uses a non-selective adiabatic BIR-4 tip-down pulse with a 2D restoration pulse (i.e. a “mirrored” version of our 2D-T_2-Prep). The advantage of this approach includes that it benefits from a more homogenous excitation through the use of an adiabatic tip-down pulse. Additionally, there is a shorter 2D pulse duration, which is achieved by exploiting a the conjugate symmetry described by Smith and Nayak (67). This short 2D pulse duration may therefore make it more robust to signal loss during the 2D pulse in regions with very short T_2* values (e.g. lung parenchyma), as lung imaging has recently been proposed as an application for self-navigated sequences (68). However, a limitation of Luo's variant is that tissues experience T_1 recovery throughout the duration of the T_2-Prep time. This may make it less suitable for longer T_2-Prep durations, as background signal recovery will reduce the benefits gained from outer volume suppression.

Note that the improvement of the 2D-T_2-Prep (vs Conventional T_2-Prep) on vessel sharpness was 34% RCA / 21% LCA (39.3 vs. 29.3 / 35.7 vs. 29.4) when using the automated segmentation approach, whereas it was only 23% RCA / 20% LCA (41.2 vs. 33.7 / 36.7 vs. 30.6) when using the iterative, reference-independent approach. Likewise, in the blinded observer ratings of coronary image quality, 2D-T_2-Prep+SN increased the mean score by 76% (2.1 vs. 1.2) for the automated segmentation approach but only 39% (1.9 vs. 1.4) when using the iterative reconstruction. That the 2D-T_2-Prep improves performance less dramatically when using the iterative reconstruction technique is interesting. Since the iterative approach has been shown to increase vessel sharpness in patients with irregular breathing (49), it suggests that the manner in which the iterative approach improves image quality may be similar that of the 2D-T_2-Prep - namely, improved motion tracking. It also suggests that the potential benefits of the 2D-T_2-Prep on blood pool tracking may also be (partially) achievable with a more robust motion tracking strategy. Note that while the iterative approach did slightly increase vessel sharpness in this study (as compared to the automated approach), the results were not considered statistically significant. However, this might be expected, as only healthy volunteers were studied in this work and the iterative approach has only been shown to improve VS in patients. Conversely, this may highlight another weakness in this study - that no patients were studied. It would certainly be interesting to see how the effects reported here translate to a patient population with irregular breathing.

Though a comparison to the reference standard Cartesian navigator-gated coronary MRA was not the focus of this study, an unpaired comparison between the above approach and a previously established whole-heart protocol (61) was performed. A paired comparison may ultimately be more meaningful, but it remains challenging to define an adequate navigator-gated (or even self-gated) Cartesian protocol with similar imaging parameters (isotropic spatial resolution, temporal resolution, volumetric coverage, etc…) to a self-navigated 3D radial sequence; this remains a lasting complication (69). Scan times for conventional, navigator-gated Cartesian approaches are unpredictable, as they depend on the respiratory pattern of a given subject. For self-navigation, however, this is not the case and the only determinant for scan time is heart rate. Nonetheless, as shown in this work, a traditional Cartesian acquisition may sometimes provide superior image quality. Additionally, in

Cartesian acquisitions, static tissue coming from either the chest wall or arms (although not simultaneously) can be avoided by limiting the FoV. A full investigation into the relative benefits of these approaches would certainly be worthwhile, but is beyond the scope of this study.

Finally, much work has recently been done with compressed sensing (CS) (70-72). With the increased sparsity introduced by the 2D-T_2-Prep, there exists a strong potential to exploit this for self-navigation purposes, such as in the case of free-running self-navigation (11,73).

Conclusion

Image quality in self-navigated 3D radial coronary MRA has been shown to significantly improve with the introduction of a 2D-T_2-Prep relative to the conventional T_2-Prep. These results have been demonstrated in both a moving phantom and through in vivo MRA of the coronary arteries in healthy volunteers. Motion detection and correction have also been shown to improve with the 2D-T_2-Prep in a moving phantom, which may contribute to the improved image quality found in vivo. The above technique should thus be considered for use in self-navigated cardiac imaging, and perhaps explored for any form of image acquisition where a local ROI is targeted and information from adjacent tissues is not required.

Supplementary Material

Refer to Web version on PubMed Central for supplementary material.

Acknowledgments

This work was in part supported by the Swiss National Science Foundation grants #P2LAP3_164909, #320030_143923, #326030_150828, and #PZ00P3-154719, as well as NIH Research Project grants R01HL094557 and R01DK098503. Additional support was provided in part by the Centre d'Imagerie BioMedical (CIBM) of the UNIL, EPFL, UNIGE, CHUV, and HUG, as well as the Jeantet and Leenaards Foundations. We would also like to thank Drs. Jessica Bastiaansen and Jerome Yerly for their insightful discussions regarding the subject matter, and Prof. Nicole Seiberlich for her current postdoctoral supervision.

References

1. van Heeswijk RB, Bonanno G, Coppo S, Coristine A, Kober T, Stuber M. Motion compensation strategies in magnetic resonance imaging. Critical Reviews™ in Biomedical Engineering. 2012; 40(2)
2. Stuber M, Weiss RG. Coronary magnetic resonance angiography. Journal of magnetic resonance imaging : JMRI. 2007; 26(2):219–234. [PubMed: 17610288]
3. Henningsson M, Botnar RM. Advanced respiratory motion compensation for coronary MR angiography. Sensors. 2013; 13(6):6882–6899. [PubMed: 23708271]
4. Hofman MB, Wickline SA, Lorenz CH. Quantification of in-plane motion of the coronary arteries during the cardiac cycle: implications for acquisition window duration for MR flow quantification. Journal of magnetic resonance imaging : JMRI. 1998; 8(3):568–576. [PubMed: 9626870]
5. Duerinckx A, Atkinson DP. Coronary MR angiography during peak-systole: work in progress. Journal of magnetic resonance imaging : JMRI. 1997; 7(6):979–986. [PubMed: 9400840]
6. Larson AC, White RD, Laub G, McVeigh ER, Li D, Simonetti OP. Self-gated cardiac cine MRI. Magnetic Resonance in Medicine. 2004; 51(1):93–102. [PubMed: 14705049]

7. Nijm GM, Sahakian AV, Swiryn S, Carr JC, Sheehan JJ, Larson AC. Comparison of self-gated cine MRI retrospective cardiac synchronization algorithms. Journal of Magnetic Resonance Imaging. 2008; 28(3):767–772. [PubMed: 18777546]
8. Krämer M, Herrmann KH, Biermann J, Reichenbach JR. Retrospective reconstruction of cardiac cine images from golden-ratio radial MRI using one-dimensional navigators. Journal of Magnetic Resonance Imaging. 2014; 40(2):413–422. [PubMed: 24895008]
9. Kolbitsch C, Prieto C, Schaeffter T. Cardiac functional assessment without electrocardiogram using physiological self-navigation. Magnetic Resonance in Medicine. 2014; 71(3):942–954. [PubMed: 23568768]
10. Ingle RR, Santos JM, Overall WR, McConnell MV, Hu BS, Nishimura DG. Self-gated fat-suppressed cardiac cine MRI. Magnetic Resonance in Medicine. 2015; 73(5):1764–1774. [PubMed: 24806049]
11. Pang J, Sharif B, Fan Z, Bi X, Arsanjani R, Berman DS, Li D. ECG and navigator-free four-dimensional whole-heart coronary MRA for simultaneous visualization of cardiac anatomy and function. Magnetic Resonance in Medicine. 2014; 72(5):1208–1217. [PubMed: 25216287]
12. Jahnke C, Paetsch I, Nehrke K, Schnackenburg B, Bornstedt A, Gebker R, Fleck E, Nagel E. A new approach for rapid assessment of the cardiac rest period for coronary MRA. Journal of Cardiovascular Magnetic Resonance. 2005; 7(2):395–399. [PubMed: 15881520]
13. Ehman RL, Felmlee JP. Adaptive technique for high-definition MR imaging of moving structures. Radiology. 1989; 173(1):255–263. [PubMed: 2781017]
14. Sinkus R, Börnert P. Motion pattern adapted real-time respiratory gating. Magnetic Resonance in Medicine. 1999; 41(1):148–155. [PubMed: 10025623]
15. Jhooti P, Gatehouse P, Keegan J, Bunce N, Taylor A, Firmin D. Phase ordering with automatic window selection (PAWS): a novel motion-resistant technique for 3D coronary imaging. Magnetic Resonance in Medicine. 2000; 43(3):470–480. [PubMed: 10725891]
16. Wang Y, Grimm RC, Felmlee JP, Riederer SJ, Ehman RL. Algorithms for extracting motion information from navigator echoes. Magn Reson Med. 1996; 36(1):117–123. [PubMed: 8795030]
17. Taylor AM, Jhooti P, Firmin DN, Pennell DJ. Automated monitoring of diaphragm end-expiratory position for real-time navigator echo MR coronary angiography. Journal of Magnetic Resonance Imaging. 1999; 9(3):395–401. [PubMed: 10194709]
18. Stuber M, Botnar RM, Danias PG, Kissinger KV, Manning WJ. Submillimeter three-dimensional coronary MR angiography with real-time navigator correction: comparison of navigator locations. Radiology. 1999; 212(2):579–587. [PubMed: 10429721]
19. Spuentrup E, Manning WJ, Botnar RM, Kissinger KV, Stuber M. Impact of navigator timing on free-breathing submillimeter 3D coronary magnetic resonance angiography. Magn Reson Med. 2002; 47(1):196–201. [PubMed: 11754460]
20. Nehrke K, Bornert P, Manke D, Bock JC. Free-breathing cardiac MR imaging: study of implications of respiratory motion--initial results. Radiology. 2001; 220(3):810–815. [PubMed: 11526286]
21. Wang Y, Riederer SJ, Ehman RL. Respiratory motion of the heart: kinematics and the implications for the spatial resolution in coronary imaging. Magn Reson Med. 1995; 33(5):713–719. [PubMed: 7596276]
22. Bracewell R. The Fourier Transform and its Applications. New York. 1965
23. Stehning C, Börnert P, Nehrke K, Eggers H, Stuber M. Free-breathing whole-heart coronary MRA with 3D radial SSFP and self-navigated image reconstruction. Magnetic Resonance in Medicine. 2005; 54(2):476–480. [PubMed: 16032682]
24. Piccini D, Littmann A, Nielles-Vallespin S, Zenge MO. Respiratory self-navigation for whole-heart bright-blood coronary MRI: Methods for robust isolation and automatic segmentation of the blood pool. Magnetic Resonance in Medicine. 2012; 68(2):571–579. [PubMed: 22213169]
25. Henningsson M, Koken P, Stehning C, Razavi R, Prieto C, Botnar RM. Whole-heart coronary MR angiography with 2D self-navigated image reconstruction. Magnetic Resonance in Medicine. 2012; 67(2):437–445. [PubMed: 21656563]

26. Lai P, Larson AC, Park J, Carr JC, Li D. Respiratory self-gated four-dimensional coronary MR angiography: A feasibility study. Magnetic Resonance in Medicine. 2008; 59(6):1378–1385. [PubMed: 18506786]
27. Bhat H, Ge L, Nielles-Vallespin S, Zuehlsdorff S, Li D. 3D radial sampling and 3D affine transform-based respiratory motion correction technique for free-breathing whole-heart coronary MRA with 100% imaging efficiency. Magnetic Resonance in Medicine. 2011; 65(5):1269–1277. [PubMed: 21500255]
28. Pang J, Bhat H, Sharif B, Fan Z, Thomson LEJ, LaBounty T, Friedman JD, Min J, Berman DS, Li D. Whole-heart coronary MRA with 100% respiratory gating efficiency: Self-navigated three-dimensional retrospective image-based motion correction (TRIM). Magnetic Resonance in Medicine. 2014; 71(1):67–74. [PubMed: 23401157]
29. Lai P, Larson AC, Bi X, Jerecic R, Li D. A dual-projection respiratory self-gating technique for whole-heart coronary MRA. Journal of Magnetic Resonance Imaging. 2008; 28(3):612–620. [PubMed: 18777542]
30. Piccini D, Bonanno G, Ginami G, Littmann A, Zenge MO, Stuber M. Is there an optimal respiratory reference position for self-navigated whole-heart coronary MR angiography? Journal of Magnetic Resonance Imaging. 2016; 43(2):426–433. [PubMed: 26174582]
31. Cruz G, Atkinson D, Buerger C, Schaeffter T, Prieto C. Accelerated motion corrected three-dimensional abdominal MRI using total variation regularized SENSE reconstruction. Magnetic Resonance in Medicine. 2015
32. Mendes J, Kholmovski E, Parker DL. Rigid-body motion correction with self-navigation MRI. Magnetic Resonance in Medicine. 2009; 61(3):739–747. [PubMed: 19097240]
33. Paschke NK, Dössel O, Schaeffter T, Prieto C, Kolbitsch C. Comparison of image-based and reconstruction-based respiratory motion correction for golden radial phase encoding coronary MR angiography. Journal of Magnetic Resonance Imaging. 2015; 42(4):964–971. [PubMed: 25639861]
34. Cruz G, Atkinson D, Henningsson M, Botnar RM, Prieto C. Highly efficient nonrigid motion-corrected 3D whole-heart coronary vessel wall imaging. Magnetic Resonance in Medicine. 2016
35. Moghari MH, Roujol S, Chan RH, Hong SN, Bello N, Henningsson M, Ngo LH, Goddu B, Goepfert L, Kissinger KV, Manning WJ, Nezafat R. Free-Breathing 3D Cardiac MRI Using Iterative Image-Based Respiratory Motion Correction. Magnetic Resonance in Medicine. 2013; 70(4):1005–1015. [PubMed: 23132549]
36. Piccini D, Monney P, Sierro C, Coppo S, Bonanno G, van Heeswijk RB, Chaptinel J, Vincenti G, de Blois J, Koestner SC. Respiratory self-navigated postcontrast whole-heart coronary MR angiography: initial experience in patients. Radiology. 2014; 270(2):378–386. [PubMed: 24471387]
37. Monney P, Piccini D, Rutz T, Vincenti G, Coppo S, Koestner SC, Sekarski N, Di Bernardo S, Bouchardy J, Stuber M. Single centre experience of the application of self navigated 3D whole heart cardiovascular magnetic resonance for the assessment of cardiac anatomy in congenital heart disease. Journal of Cardiovascular Magnetic Resonance. 2015; 17(1):1–12. [PubMed: 25589308]
38. Henningsson M, Hussain T, Vieira MS, Greil GF, Smink J, Beck G, Botnar RM. Whole-heart coronary MR angiography using image-based navigation for the detection of coronary anomalies in adult patients with congenital heart disease. Journal of Magnetic Resonance Imaging. 2015
39. He Y, Pang J, Dai Q, Fan Z, An J, Li D. Diagnostic Performance of Self-navigated Whole-Heart Contrast-enhanced Coronary 3-T MR Angiography. Radiology. 2016; 152514
40. Glover G, Pauly J. Projection reconstruction techniques for reduction of motion effects in MRI. Magnetic Resonance in Medicine. 1992; 28(2):275–289. [PubMed: 1461126]
41. Feinberg DA, Hoenninger JC, Crooks LE, Kaufman L, Watts JC, Arakawa M. Inner volume MR imaging: technical concepts and their application. Radiology. 1985; 156(3):743–747. [PubMed: 4023236]
42. Bottomley PA. Spatial Localization in NMR Spectroscopy in Vivo. Annals of the New York Academy of Sciences. 1987; 508(1):333–348. [PubMed: 3326459]
43. Frahm J, Merboldt KD, Hänicke W. Localized proton spectroscopy using stimulated echoes. Journal of Magnetic Resonance (1969). 1987; 72(3):502–508.

44. Bottomley PA, Hardy CJ. Two-dimensional spatially selective spin inversion and spin-echo refocusing with a single nuclear magnetic resonance pulse. J Appl Phys. 1987; 62(10):4284–4290.
45. Abd-Elmoniem KZ, Barmet C, Stuber M. Free-breathing inner-volume black-blood imaging of the human heart using two-dimensionally selective local excitation at 3 T. Magnetic Resonance in Medicine. 2012; 68(3):822–829. [PubMed: 22161817]
46. Coristine AJ, van Heeswijk RB, Stuber M. Combined T2-preparation and two-dimensional pencil-beam inner volume selection. Magnetic Resonance in Medicine. 2015; 74(2):529–536. [PubMed: 25163988]
47. Coristine AJ, Yerly J, Stuber M. A Cylindrical, Inner Volume Selecting 2D-T 2-Prep Improves GRAPPA-Accelerated Image Quality in MRA of the Right Coronary Artery. PloS one. 2016; 11(10):e0163618. [PubMed: 27736866]
48. Piccini D, Littmann A, Nielles-Vallespin S, Zenge MO. Spiral phyllotaxis: The natural way to construct a 3D radial trajectory in MRI. Magnetic Resonance in Medicine. 2011; 66(4):1049–1056. [PubMed: 21469185]
49. Ginami G, Bonanno G, Schwitter J, Stuber M, Piccini D. An iterative approach to respiratory self-navigated whole-heart coronary MRA significantly improves image quality in a preliminary patient study. Magnetic Resonance in Medicine. 2015; doi: 10.1002/mrm.25761
50. Brittain JH, Hu BS, Wright GA, Meyer CH, Macovski A, Nishimura DG. Coronary angiography with magnetization-prepared T_2 contrast. Magn Reson Med. 1995; 33(5):689–696. [PubMed: 7596274]
51. Pauly JM, Nishimura DG, Macovski A. A k-space analysis of small-tip-angle excitation. J Magn Reson. 1989; 81:43–56.
52. Pauly JM, Nishimura DG, Macovski A. A linear class of large-tip-angle selective excitation pulses. J Magn Reson. 1989; 82:571–587.
53. Nehrke K, Bornert P, Groen J, Smink J, Bock JC. On the performance and accuracy of 2D navigator pulses. Magn Reson Imaging. 1999; 17(8):1173–1181. [PubMed: 10499679]
54. Börnert P, Aldefeld B. On spatially selective RF excitation and its analogy with spiral MR image acquisition. Magnetic Resonance Materials in Physics, Biology and Medicine. 1998; 7(3):166–178.
55. Hardy CJ, Cline HE. Broadband nuclear magnetic resonance pulses with two-dimensional spatial selectivity. J Appl Phys. 1989; 66:1513.
56. van Heeswijk RB, Feliciano H, Bongard C, Bonanno G, Coppo S, Lauriers N, Locca D, Schwitter J, Stuber M. Free-Breathing 3 T Magnetic Resonance T_2-Mapping of the Heart. JACC: Cardiovascular Imaging. 2012; 5(12):1231–1239. [PubMed: 23236973]
57. van Heeswijk RB, Piccini D, Feliciano H, Hullin R, Schwitter J, Stuber M. Self-navigated isotropic three-dimensional cardiac T2 mapping. Magnetic Resonance in Medicine. 2015; 73(4):1549–1554. [PubMed: 24809849]
58. Hwang TL, van Zijl PC, Garwood M. Fast broadband inversion by adiabatic pulses. J Magn Reson. 1998; 133(1):200–203. [PubMed: 9654487]
59. Huber ME, Stuber M, Botnar RM, Boesiger P, Manning WJ. Low-cost MR-compatible moving heart phantom. Journal of Cardiovascular Magnetic Resonance. 2000; 2(3):181–187. [PubMed: 11545115]
60. Etienne A, Botnar RM, Van Muiswinkel AM, Boesiger P, Manning WJ, Stuber M. “Soap-Bubble” visualization and quantitative analysis of 3D coronary magnetic resonance angiograms”. Magn Reson Med. 2002; 48(4):658–666. [PubMed: 12353283]
61. Sakuma H, Ichikawa Y, Suzawa N, Hirano T, Makino K, Koyama N, Van Cauteren M, Takeda K. Assessment of Coronary Arteries with Total Study Time of Less than 30 Minutes by Using Whole-Heart Coronary MR Angiography 1. Radiology. 2005; 237(1):316–321. [PubMed: 16126921]
62. Prieto C, Doneva M, Usman M, Henningsson M, Greil G, Schaeffter T, Botnar RM. Highly efficient respiratory motion compensated free-breathing coronary mra using golden-step Cartesian acquisition. Journal of Magnetic Resonance Imaging. 2015; 41(3):738–746. [PubMed: 24573992]
63. Ingle RR, Wu HH, Addy NO, Cheng JY, Yang PC, Hu BS, Nishimura DG. Nonrigid autofocus motion correction for coronary MR angiography with a 3D cones trajectory. Magnetic Resonance in Medicine. 2014; 72(2):347–361. [PubMed: 24006292]

64. Forman C, Piccini D, Grimm R, Hutter J, Hornegger J, Zenge MO. Reduction of respiratory motion artifacts for free-breathing whole-heart coronary MRA by weighted iterative reconstruction. Magnetic Resonance in Medicine. 2015; 73(5):1885–1895. [PubMed: 24912763]

65. Coristine AJ, van Heeswijk RB, Stuber M. Fat signal suppression for coronary MRA at 3T using a water-selective adiabatic T2-preparation technique. Magnetic Resonance in Medicine. 2014; 72(3): 763–769. [PubMed: 24285603]

66. Luo J, Addy NO, Ingle RR, Hargreaves BA, Hu BS, Nishimura DG, Shin T. Combined outer volume suppression and T2 preparation sequence for coronary angiography. Magnetic Resonance in Medicine. 2014 n/a-n/a.

67. Smith TB, Nayak KS. Reduced field of view MRI with rapid, B1-robust outer volume suppression. Magnetic Resonance in Medicine. 2012; 67(5):1316–1323. [PubMed: 22083545]

68. Delacoste, J., Chaptinel, J., Beigelman, C., Piccini, D., Sauty, A., Stuber, M. A Double Echo Ultra Short Echo Time Acquisition for Respiratory Motion Suppressed High Resolution Imaging of the Lung. Proceedings of the 23rd Annual Meeting of ISMRM; Toronto, Ontario, Canada. 2015.

69. Henningsson M, Mens G, Koken P, Smink J, Botnar RM. A new framework for interleaved scanning in cardiovascular MR: Application to image-based respiratory motion correction in coronary MR angiography. Magnetic Resonance in Medicine. 2015; 73(2):692–696. [PubMed: 24639003]

70. Lustig M, Donoho D, Pauly JM. Sparse MRI: The application of compressed sensing for rapid MR imaging. Magnetic Resonance in Medicine. 2007; 58(6):1182–1195. [PubMed: 17969013]

71. Yerly J, Ginami G, Nordio G, Coristine AJ, Coppo S, Monney P, Stuber M. Coronary endothelial function assessment using self-gated cardiac cine MRI and k-t sparse SENSE. Magnetic Resonance in Medicine. 2015; doi: 10.1002/mrm.26050

72. Bonanno G, Puy G, Wiaux Y, van Heeswijk RB, Piccini D, Stuber M. Self-Navigation with Compressed Sensing for 2D Translational Motion Correction in Free-Breathing Coronary MRI: A Feasibility Study. PloS one. 2014; 98:e105523. 2014.

73. Coppo S, Piccini D, Bonanno G, Chaptinel J, Vincenti G, Feliciano H, van Heeswijk RB, Schwitter J, Stuber M. Free-running 4D whole-heart self-navigated golden angle MRI: Initial results. Magnetic Resonance in Medicine. 2015; 74(5):1306–1316. [PubMed: 25376772]

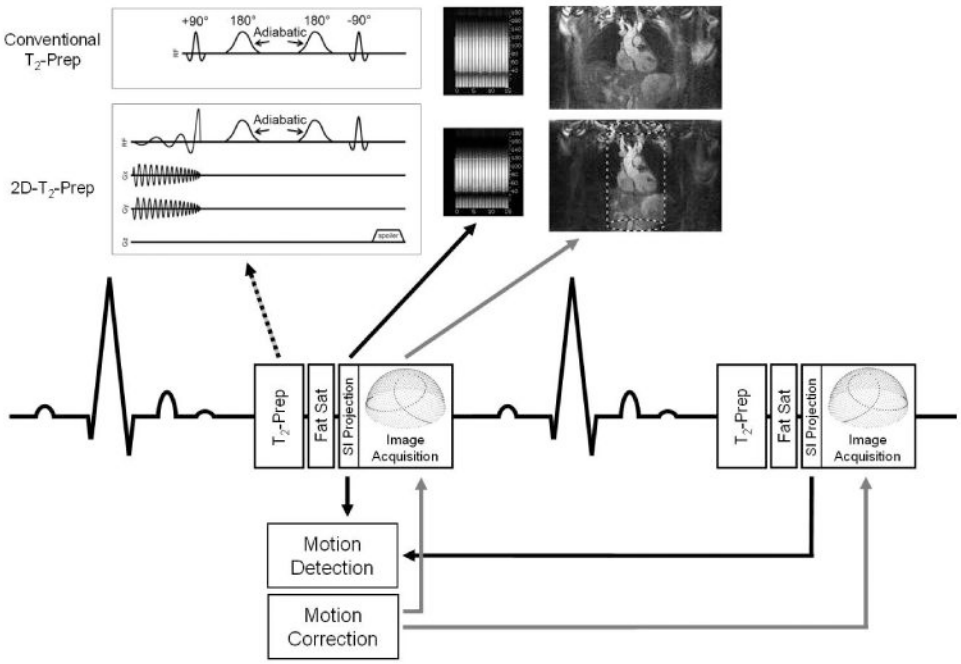

Figure 1.

Schematic diagram for the 3D radial self-navigated pulse sequences. After each heartbeat, a T_2 preparation module (dotted arrow) is played out prior to image acquisition. The cardiac blood pool is detected by segmenting a 1D SI projection (black arrow). That blood pool position is used to determine respiratory motion, which can be corrected for by applying a phase shift to the associated k-space data (gray arrows). Two T_2-Prep modules were compared: a conventional T_2-Prep (upper row) and an outer volume suppressing "2D-T_2-Prep" (lower row), where the targeted inner volume is indicated by a dashed cylinder.

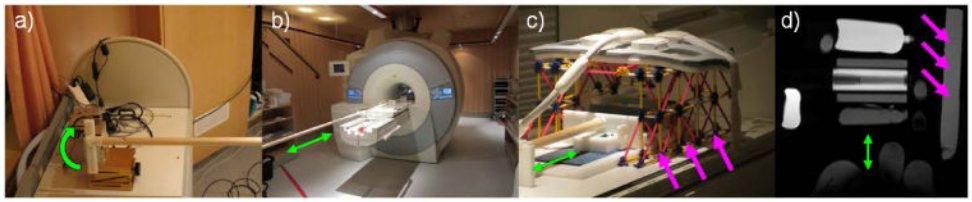

Figure 2.

Moving phantom setup. A stepper motor (a) rotates at a programmable frequency. This causes a wooden pole to move sinusoidally in and out of the scanner bore (b), driving a rolling cart (c), which can be loaded with various tissue-mimicking phantoms. By setting the stepper motor rotation to 17 RPM, respiratory motion may be simulated (green arrows, b-d). Likewise, additional phantoms may be placed in the cage structure surrounding the cart (pink arrows), to mimic static tissues such as the arms and chest wall, as seen in (c) and a corresponding MR image (d).

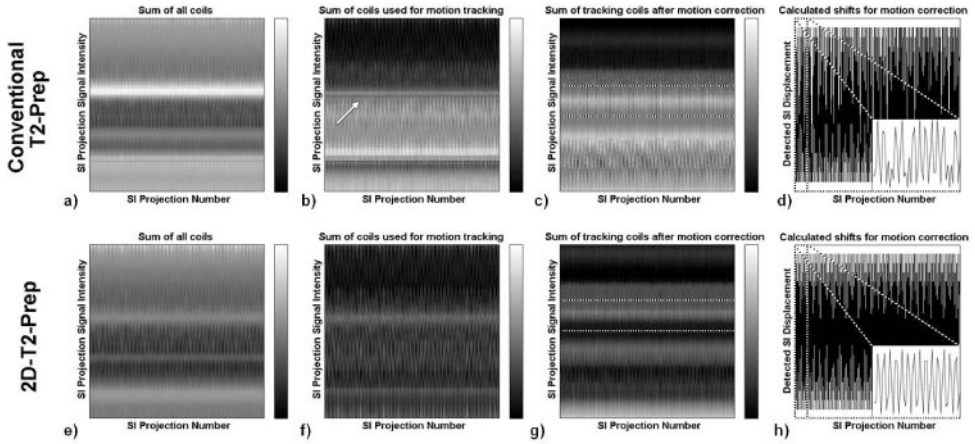

Figure 3.

Superior-Inferior (SI) projections used for self-navigation in a moving phantom. Prior to motion correction (a,e), a subset of coils are selected for motion tracking (b,f) and each 1D SI projection is iteratively shifted (c,g) to determine phantom motion. With outer volume suppression (f), static structures (white arrow, b) are suppressed. Correspondingly, the detected SI displacements (d,h) are more regularly periodic (inserts, d,h) for the 2D-T_2-Prep (h), and more closely match the expected motion.

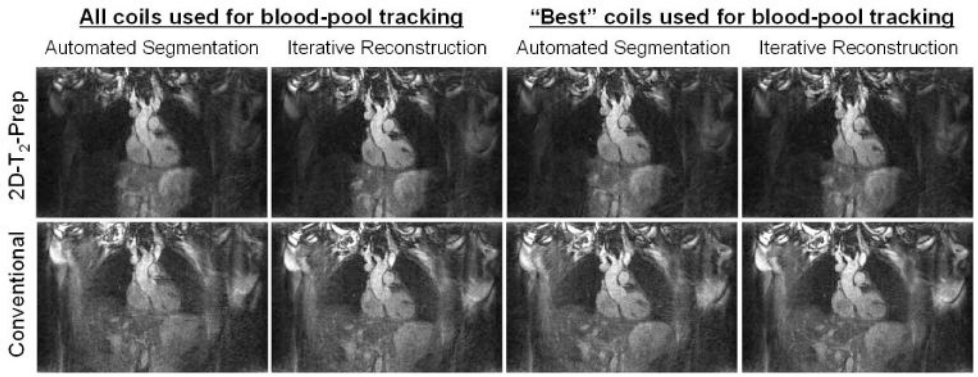

Figure 4.

Sample slices comparing the 2D-T_2-Prep (top) and its conventional counterpart (bottom). Note that regardless of the strategy used for motion correction, and regardless of the coil selection, there is an increased background signal suppression for the 2D-T_2-Prep and a corresponding reduction in streaking artefacts.

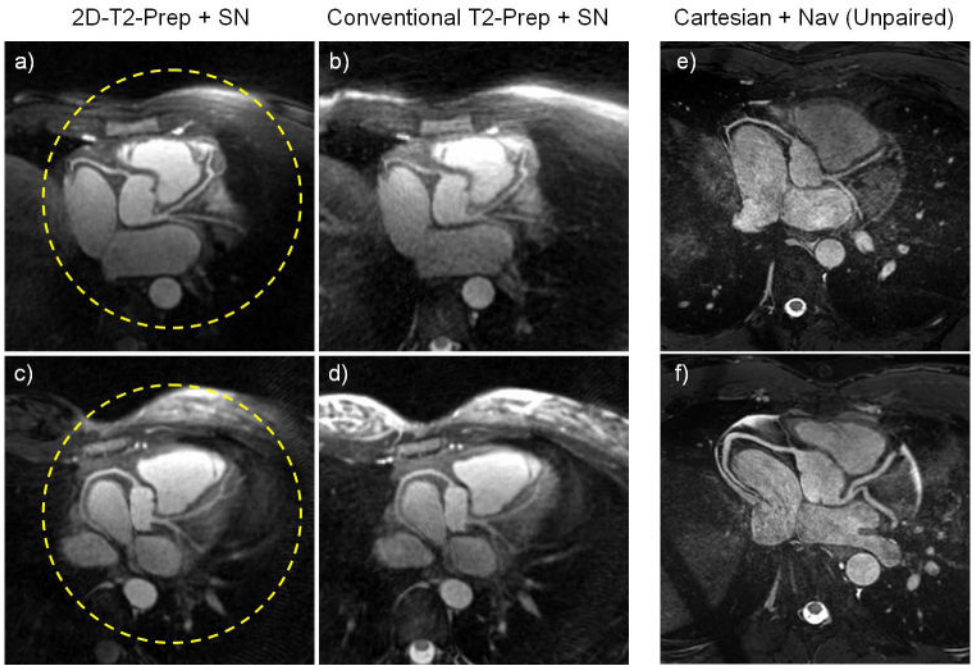

Figure 5.

Left: Coronary arteries of two volunteers after image reformatting, for both T_2-Prep techniques. The area targeted by the 2D-T_2-Prep "pencil-beam" is outlined by a dashed circle (a,c). Note the decreased background signal in the 2D-T_2-Prep (left) compared to the conventional T_2-Prep (right), as well as the increased conspicuity of the distal left coronary system for the 2D-T_2-Prep image. *Right*: Coronary artery images of two different volunteers, after image reformatting (e,f), collected in whole-heart Cartesian acquisitions. Provided for comparison to Gold-standard reference.

Table 1

Tables of SNR and CNR values in the blood, myocardium, and lungs. Note that regardless of the coil selection or reconstruction / motion tracking technique used, the 2D-T_2-Prep improves image quality.

-		SNR							
		All Coils				Best Coils			
Tissue	T2-Prep	Automated		Iterative		Automated		Iterative	
Blood	Conv. T2-Prep	18.2 ± 1.5	*0.001	18.1 ± 1.7	*0.002	18.7 ± 2.0	*0.001	18.6 ± 1.5	*0.002
	2D-T2-Prep	23.9 ± 3.6		24.1 ± 3.7		24.5 ± 3.4		24.0 ± 3.8	
Myocardium	Conv. T2-Prep	8.6 ± 1.6	*0.02	8.6 ± 1.8	*0.02	9.0 ± 2.0	*0.05	8.6 ± 1.6	*0.02
	2D-T2-Prep	10.7 ± 2.5		10.6 ± 2.6		10.3 ± 1.7		10.2 ± 2.0	
Lungs	Conv. T2-Prep	4.5 ± 0.4	*0.05	4.4 ± 0.4	*0.02	4.6 ± 0.4	*0.005	4.5 ± 0.3	*0.002
	2D-T2-Prep	3.8 ± 0.3		3.7 ± 0.3		3.7 ± 0.3		3.6 ± 0.3	
			*p<		*p<		*p<		*p<

-		CNR							
		All Coils				Best Coils			
Contrast	T2-Prep	Automated		Iterative		Automated		Iterative	
Blood-Myocardium	Conv. T2-Prep	9.6 ± 1.3	*0.001	9.5 ± 1.3	*0.002	9.7 ± 1.2	*0.005	10.0 ± 1.4	*0.002
	2D-T2-Prep	13.2 ± 2.5		13.4 ± 3.2		14.2 ± 2.8		13.8 ± 2.9	
Blood- Lung	Conv. T2-Prep	13.7 ± 1.3	*0.001	13.7 ± 1.5	*0.001	14.1 ± 1.7	*0.001	14.1 ± 1.4	*0.001
	2D-T2-Prep	20.1 ± 3.4		20.4 ± 3.4		20.8 ± 3.2		20.4 ± 3.5	
Myocardium-Lung	Conv. T2-Prep	4.1 ± 1.4	*0.002	4.2 ± 1.6	*0.005	4.4 ± 1.7	*0.001	4.1 ± 1.5	*0.001
	2D-T2-Prep	6.9 ± 2.5		7.0 ± 2.5		6.6 ± 1.7		6.5 ± 2.0	
			*p<		*p<		*p<		*p<

Note: All values are ± standard deviation.